Internal distribution of Li and B in serpentinites from the Feather River Ophiolite, California based on laser ablation ICP-MS

Cin-Ty Aeolus Lee, Masaru Oka, Peter Luffi, Arnaud Agranier

Geochemistry Geophysics Geosystems G3
AN ELECTRONIC JOURNAL OF THE EARTH SCIENCES
Published by AGU and the Geochemical Society

Article
Volume 9, Number 12
6 December 2008
Q12011, doi:10.1029/2008GC002078
ISSN: 1525-2027

Internal distribution of Li and B in serpentinites from the Feather River Ophiolite, California, based on laser ablation inductively coupled plasma mass spectrometry

Cin-Ty Aeolus Lee, Masaru Oka, and Peter Luffi
Department of Earth Science, Rice University, MS-126, 6100 Main Street, Houston, Texas 77005, USA (ctlee@rice.edu)

Arnaud Agranier
Department of Earth Science, Rice University, MS-126, 6100 Main Street, Houston, Texas 77005, USA

Institut Universitaire Europeen de la Mer, Universite de Bretagne Occidentale, UMR6538, CNRS, F-29238 Brest CEDEX 3, France

[1] Laser ablation inductively coupled plasma mass spectrometry (LA-ICP-MS) analyses of B and Li in serpentinized peridotites from the Feather River Ophiolite (California) indicates that B is enriched in serpentine minerals compared to the whole-rock and less altered olivine grains, while Li in serpentine is depleted or comparable to whole-rock Li. The high B contents of serpentine minerals correlate with the relatively enriched whole-rock B contents. The low Li contents of serpentine minerals are consistent with the relatively low Li whole-rock contents and suggest that only small amounts of Li were added during serpentinization or that some Li was even leached out. A simple model of partial melting shows that Li/Yb increases with increasing melt depletion (and clinopyroxene depletion) in the peridotitic residue because Li is most compatible in olivine while Yb is most compatible in clinopyroxene. Thus, high Li/Yb ratios in peridotites by themselves do not indicate secondary enrichments in Li. However, Li/Yb and Yb contents of many of the Feather River Ophiolites plot above the melt depletion curve in Li/Yb versus Yb space, indicating that these serpentinites experienced subtle and preferential enrichments in Li during serpentinization. If serpentinized oceanic lithospheric mantle, as represented by the Feather River Ophiolite, is important in subduction recycling, then recycled mantle domains having a serpentinite protolith might be characterized by strong B enrichments but only small Li enrichments.

Components: 8156 words, 5 figures, 1 table.

Keywords: lithium; boron; serpentinite; serpentine; ultramafic; ophiolite.

Index Terms: 1065 Geochemistry: Major and trace element geochemistry.

Received 28 April 2008; **Revised** 20 October 2008; **Accepted** 28 October 2008; **Published** 6 December 2008.

Lee, C.-T. A., M. Oka, P. Luffi, and A. Agranier (2008), Internal distribution of Li and B in serpentinites from the Feather River Ophiolite, California, based on laser ablation inductively coupled plasma mass spectrometry, *Geochem. Geophys. Geosyst.*, *9*, Q12011, doi:10.1029/2008GC002078.

1. Introduction

[2] When ultramafic rocks (olivine + pyroxene), such as peridotites, react with water at low to intermediate temperatures (<700°C), the end product is a rock composed of various hydrous magnesian silicates, such as serpentines, brucites, talc, and chlorites [*Evans*, 1977; *Seyfried and Dibble*, 1980; *Bonatti et al.*, 1984; *Janecky and Seyfried*, 1986]. Such rocks are generically called serpentinites. Serpentinites can form in many types of geologic environments. In ocean basins, low-temperature serpentinization (<100°C) in the form of weathering occurs where lithospheric mantle peridotites are exhumed directly to the seawater-crust interface (e.g., in the form of abyssal peridotites [*Snow and Dick*, 1995]), such as might occur in slow-spreading ridges and along fractures [*Escartin et al.*, 1997]. Serpentinization can also occur by hydrothermal (>100 C) circulation or penetration of seawater deep (kilometer-scale) into the oceanic lithosphere at mid-ocean ridges and along fracture zones and faults [*Seyfried and Dibble*, 1980; *Janecky and Seyfried*, 1986]. These serpentinized lithospheres appear to be recycled back into the mantle when the oceanic lithosphere subducts [*Hacker et al.*, 2003; *Ranero et al.*, 2003; *Li and Lee*, 2006; *Brudzinski et al.*, 2007]. Finally, deep serpentinization can also occur in the corner of the mantle wedge when dehydrating fluids released from the top of the subducting slab infiltrate the base of the overriding lithosphere [*Bostock et al.*, 2002].

[3] The presence of serpentinites may be important in the evolution of planets with a watery surface, such as Earth [*Lee and Chen*, 2007; *Lee et al.*, 2008]. For example, serpentinized oceanic lithospheric mantle may represent the primary mechanism by which water is transported into the Earth's deep interior [*Rüpke et al.*, 2004]. Water, in turn, lowers the viscosity of the Earth's mantle and promotes melting at subduction zones [*Hirth and Kohlstedt*, 1996; *Hirth and Kohlstedt*, 2004; *Grove et al.*, 2006] and hence is critical to our understanding of mantle convection and the genesis of continental crust. Serpentinites are also unusual in that they are considerably less dense and much weaker than their unhydrated peridotite protoliths [*Hilairet et al.*, 2007]. The lower density means that extensive serpentinization of oceanic lithosphere could partially compensate for the thermally imparted negative buoyancy of subducting oceanic lithosphere while the weak rheology means that serpentinized layers and zones in oceanic or continental lithospheres could serve as weak fault zones along which deformation is accommodated [*Cooper et al.*, 2006; *Hilairet et al.*, 2007; *Lee and Chen*, 2007; *Lee et al.*, 2008].

[4] Serpentine minerals dehydrate upon heating and break down into strong, nominally anhydrous minerals, such as olivine. For example, the most stable serpentine mineral, antigorite, breaks down at ~600–700°C [*Evans et al.*, 1976; *Evans*, 1977], which means that the "lubricating" properties of serpentinites can only operate at temperatures lower than this breakdown temperature. This property led some of us to hypothesize that serpentinites were instrumental in making the thick continental lithospheric mantle (~200 km) underlying Archean cratons [*Lee et al.*, 2008]. We hypothesized that the upper serpentinized zone of oceanic lithospheric mantle allowed for the development of a weak fault zone, which then facilitated oceanic lithospheres to be thrust-stacked upon each other. However, once the fault zones heat up by thermal diffusion, the serpentinites break down, strengthening and healing the fault zone. This combination of initially weak properties followed by strengthening could explain how thick cratonic mantle is formed [*Cooper et al.*, 2006]. Although still speculative, the notion of serpentine playing a role in continent formation appears to be growing [*Canil*, 2008].

[5] All of the above proposed roles for serpentinites in deep Earth processes need to be tested. One way to test for the past role of serpentinites is to identify those geochemical signatures that are imprinted during hydrothermal serpentinization but might survive the dehydration reactions associated with metamorphism during subduction or tectonic emplacement. For example, serpentinization is known to modify major and trace element systematics due to dissolution of certain major elements and to reaction and contamination of the ultramafic protolith by seawater [*Bonatti et al.*, 1984; *Snow and Dick*, 1995; *Leeman and Sisson*, 1996; *Seyfried et al.*, 1998; *Tenthorey and Hermann*, 2004; *Li and Lee*, 2006; *Agranier et al.*, 2007]. Serpentinization may lead to oxygen isotopic signatures that deviate significantly from the mantle [*Bonatti et al.*, 1984; *Gao et al.*, 2006]. Serpentinites may also be highly enriched in B and Li because these elements are enriched in seawater and hydrothermal fluids due to their high solubilities in aqueous fluids [*Bonatti et al.*, 1984; *Scambelluri*

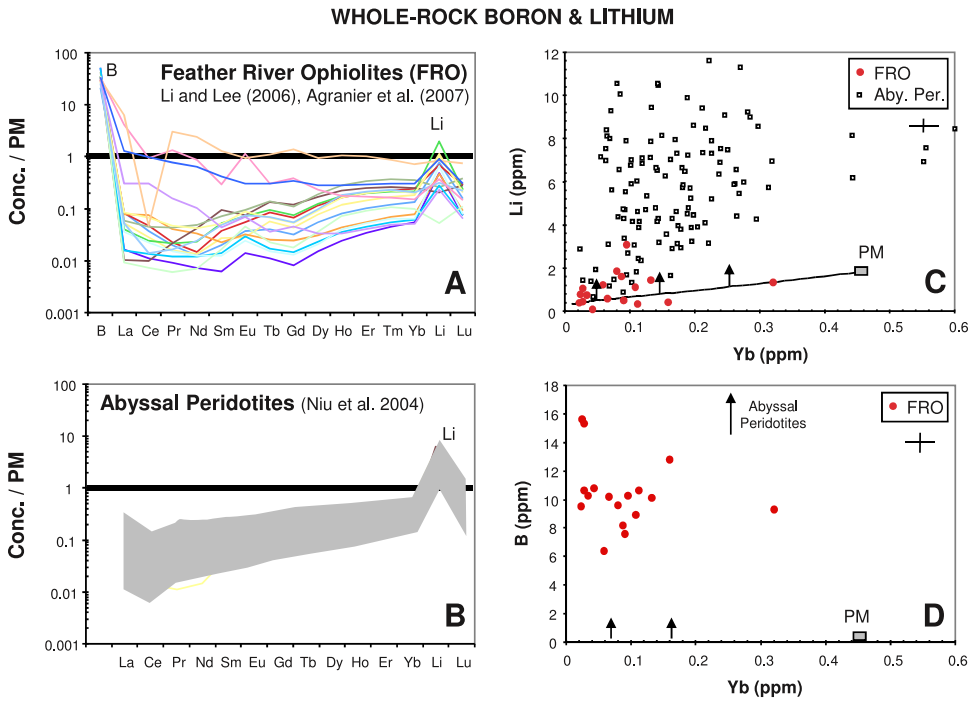

Figure 1. Compilation of whole-rock data from *Agranier et al.* [2007] and *Li and Lee* [2006] compared to literature data. (a) Boron, lithium, and rare earth element data for Feather River Ophiolites (FRO) normalized to primitive mantle (PM). Note high enrichment in B and high Li/Yb ratios. (b) Abyssal peridotite data for Li and rare earth elements from *Niu* [2004]. Note high Li/Yb ratios. (c) Whole-rock Li versus Yb in FRO peridotites and abyssal peridotites from *Niu* [2004]. Diagonal line represents melt depletion line (see text for details). (d) B versus Yb from *Agranier et al.* [2007]. Arrows point in direction of serpentinization. Crosses in Figures 1c and 1d represent 2 standard error uncertainties.

et al., 2001; *Decitre et al.*, 2002; *Savov et al.*, 2005a; *Scambelluri et al.*, 2004; *Savov et al.*, 2005b]. Interestingly, *Scambelluri et al.* [2004] showed that not only have serpentinized ophiolites been enriched in B and Li, but much of this B and Li was retained during prograde metamorphism, that is, beyond antigorite breakdown at ~600°C. If some of the original serpentinite B and Li can be retained, then B and Li could be used to identify peridotites that have had a serpentinization history. To expand on these suggestions, we combine micron-scale distributions of B and Li in partially serpentinized peridotites from the Feather River Ophiolite in northern California with previously published whole-rock compositions on the same rocks. Our results are consistent with B being elevated in serpentine minerals to levels far in excess of unaltered olivines and pyroxenes. In contrast, we show that the least altered olivines and pyroxenes have equal or higher Li contents than serpentine minerals, suggesting that Li is not always as good a tracer of serpentine as B. Nevertheless, serpentinites are still enriched in Li and we provide some guidelines for quantifying these enrichment levels.

2. Feather River Ophiolite, California, and Sample Descriptions

[6] The Feather River ophiolite (FRO) is a north-south trending belt of variably serpentinized ultramafic rocks, which form part of the Sierran metamorphic foothills along the west flank of the Sierra Nevada batholith in California [*Day et al.*, 1985; *Hacker and Peacock*, 1990; *Mayfield and Day*, 2000]. The peridotitic precursors of the serpentinites were mostly residual harzburgites based on high MgO contents, low Al_2O_3 contents, high Cr/(Cr+Al) ratios, and extremely depleted light rare earth abundance patterns [*Li and Lee*, 2006] (Figure 1a). The degree of serpentinization varies from ~50% to 100% serpentinization based on petrographic examination; samples that have not been completely serpentinized preserve some relatively unaltered olivine and pyroxene grains set within a serpentinite matrix but even these relict

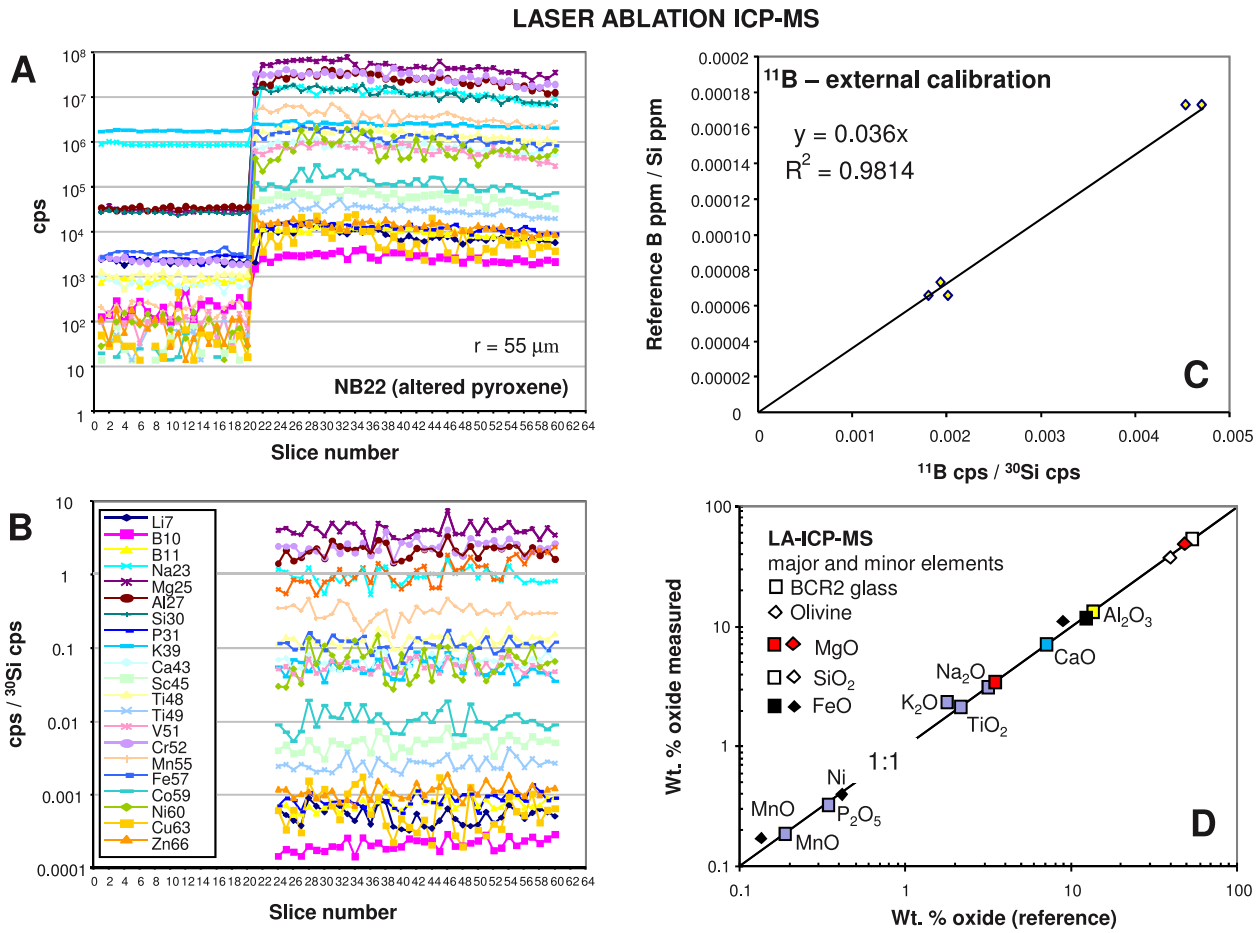

Figure 2. Technical details. (a) Example of a time-resolved signal for laser ablation inductively coupled plasma mass spectrometry (LA-ICP-MS), including background and sample analysis (sample NB22). (b) Example of internal standard-normalized elemental signals after subtracting background for same sample as in Figure 2a. Parallel nature of each isotope signal implies homogeneity on the length-scales of ablation (100 microns). (c) External calibration curve for Figure 2b using two obsidian glass standards. (d) Major and minor element data for U. S. Geological Survey BCR2g (basaltic glass) and olivine (Grand Canyon mantle xenoliths) as determined by medium mass resolution LA-ICP-MS and calculated by assuming elemental oxides add up to 100%. Diagonal line represents 1:1 line between measured/calculated and accepted compositions based on electron microprobe analyses.

grains show microscopic evidence for serpentine alteration in the form of serpentinized cracks or inclusions [*Li and Lee*, 2006]. Serpentine minerals are probably dominated by lizardite and chrysotile (based on the presence of asbestos texture and lack of massive, blocky serpentine in field outcrop), suggesting that metamorphic temperatures did not exceed the breakdown temperature of chrysotile (~350°C).

[7] Although the FRO has been interpreted to represent both subarc and oceanic lithospheric mantle, in a recent petrologic and geochemical study of the FRO in the vicinity of the Sugar Pine Reservoir area [*Mayfield and Day*, 2000], we reported a seawater trace element signature (enrichments in Cs, U, Sr) rather than those (e.g., low Nb/La ratio) thought to be typical of arcs [*Li and Lee*, 2006]. It was also shown that the serpentinization process of the FRO differed fundamentally from the low-temperature weathering serpentinization characterizing abyssal peridotites [*Li and Lee*, 2006]. Weathering serpentinization is associated with direct exposure of ultramafic rocks to the ocean, resulting in high integrated water/rock ratios, extensive loss of Mg, and complete overprinting by seawater Os isotopes. In contrast, the FRO serpentinites show much less disturbance in major element and Os isotopic compositions, which led to the hypothesis that the FRO serpentinites instead formed by infiltration of seawater

into the deep lithosphere along fractures [*Agranier et al.*, 2007].

[8] *Agranier et al.* [2007] argued that serpentinized ophiolites, instead of serpentinized abyssal peridotites, might be more representative of the types of serpentinites being subducted into the Earth's interior because weathering serpentinization is likely to be confined to a thin (<5 km?) layer at the uppermost part of the oceanic lithosphere, whereas serpentinization along fractures could extend deeper than 10 km. Agranier et al. argued that the FRO peridotites were enriched in B and Li (Figures 1a, 1c, and 1d). Whole-rock B contents are much higher than any estimates of primitive mantle (Figure 1d) [cf. *Chaussidon and Jambon*, 1994; *Leeman and Sisson*, 1996]. Whole-rock Li contents are not distinctly elevated relative to primitive mantle estimates, but whole-rock Li/Yb ratios are elevated (Figure 1c). Li and Yb are commonly thought to behave similarly during mantle melting because the Li/Yb ratios of mid-ocean ridge basalts (MORBs) are constant and only slightly lower than primitive mantle [*Ryan and Langmuir*, 1987; *McDonough and Sun*, 1995]. Thus, anomalously high Li/Yb ratios, such as seen in arc magmas, peridotite xenoliths, peridotite massifs, and abyssal peridotites, are often explained by preferential re-enrichment of Li by high temperature metasomatic fluids or seawater [*Ottolini et al.*, 2004] (see Figures 1b and 1c). Ryan and Langmuir, however, pointed out that Li is most compatible in olivine unlike Yb, which is known to be most compatible in clinopyroxene. Thus the apparent constancy of Li/Yb in MORBs is due to the bulk partition coefficients of lherzolite melting being roughly equal for Li and Yb. While high Li/Yb values in many arc magmas are likely the result of preferential Li enrichment by fluids [*Ryan and Langmuir*, 1987], high Li/Yb ratios in peridotite residues must be interpreted with caution. We will return to this issue in section 5.

3. Methods

[9] Samples were prepared as polished thick sections (>300 microns) and represent a subset of a larger sample set previously investigated for whole-rock chemistry. All samples were washed and ultrasonicated in ethanol. In situ measurements were done by LA-ICP-MS using a New Wave 213 nm laser ablation system coupled to a Thermo-Finnigan Element 2 magnetic-sector ICP-MS at Rice University. Spot sizes of 110 microns were used in order to homogenize large areas of fine-grained serpentinite groundmass. We used a laser energy density of 15 J/cm^2 with a repetition rate of 10 Hz. The ablated material was carried out of the ablation cell with helium gas and then mixed with argon gas before entering the torch. Measurements were made in medium mass resolution mode ($m/\Delta m = 3000$) to resolve isobaric interferences of doubly charged ^{20}Ne and ^{22}Ne on ^{10}B and ^{11}B (although sensitivity drops by a factor of ~10 relative to low mass resolution) as well as interferences on the major and minor elements (Mg, Ca, Si, Na, K, Fe, Mn). Sensitivity of the instrument in medium mass resolution was 4000 cps/ppm (on La) for a spot size of 55 microns and the above laser operating conditions. Mass calibration drift was corrected for in real time by monitoring the mass offset of the $^{40}Ar^{40}Ar^{+}$ dimer and correcting the total mass calibration accordingly. Both B isotopes were measured for quality control and are reported in Table 1. Peak dwell time for ^{7}Li, ^{10}B, and ^{11}B was 0.06 s. Analyses consisted of 8 to 10 measurements (~20–30 s) of the gas background followed by 30–50 measurements (2–3 min) during ablation of the sample (Figures 2a and 2b). Gas background signals were subtracted from sample signals and background-subtracted signals were then normalized to an internal standard (^{30}Si). USGS glass standards BHVO2g, BCR2g and BIR1g were used as simultaneous external standards for all elements [*Gao et al.*, 2002] except for B, where we used three obsidian glasses whose B contents were previously determined by solution standard addition (M3–33 = 26 ppm, M3–86 = 61 ppm, and M3–79 = 23 ppm; samples are available upon request). External calibration to three different USGS standards (and obsidian glasses) departs from the traditional approach of LA-ICP-MS wherein only one external standard is used. However, the simultaneous use of several calibration standards helps to bracket the concentrations in the sample unknowns, decreasing errors associated with matrix-dependent elemental fractionations and extrapolation of calibration curve. The accuracy of the external calibrations for B is shown in Figure 2c. Concentrations determined from both B isotopes are shown in Table 1. Slight discrepancies between the two are within the error of the measurements. We attribute the slight differences to instabilities of the mass calibration in medium mass resolution where peak shapes are narrow and pointed (instead of flat-topped). We take the average of the two as representative of B concentrations. In most cases, the differences are less than 10%.

Table 1 (Sample). Individual Ablation Points [The full Table 1 is available in the HTML version of this article at http://www.g-cubed.org]

			NB22														NB10b								NB24			
			16	17	18	19	20	21	22	23	24	25	26	27	27b	28	29	30	31	32	33	34	35	36	37	38	39	40
Li	Li7	ppm	2.6	2.2	2.2	2.7	2.4	2.6	3.5	5.4	0.9	1.2	0.5	1.1	0.9	1.0	0.04	0.12	0.06	0.04	0.16	0.14	0.69	0.00	n.d.	0.2	n.d.	0.01
B	B10	ppm	7	7	8	7	7	6	8	6	5	12	9	5	7	4	42	45	19	13	25	40	19	40	49	32	25	25
B	B11	ppm	7	8	8	6	8	7	8	7	6	14	10	5	7	4	50	51	19	15	25	43	22	44	52	35	29	28
P	P31	ppm	11	9	9	11	15	15	15	13	16	10	10	19	28	10	18	52	19	10	13	17	9	14	22	23	21	18
K	K39	ppm	72	65	46	78	56	75	n.d.	1	n.d.	11	n.d.	n.d.	3	n.d.	75	7	3	3	n.d.	n.d.	33	n.d.	17	3	8	n.d.
Sc	Sc45	ppm	24	17	19	25	16	25	37	44	3	10	4	3	4	2	6	6	4	3	7	7	9	7	9.9	16	7.8	7.8
Ti	Ti49	ppm	141	88	97	149	108	167	584	654	11	74	54	12	31	6	93	69	68	71	42	72	127	92	111	114	111	119
V	V51	ppm	119	71	82	126	83	115	159	186	4	62	27	4	13	1	12	19	7	6	27	17	113	16	62	34	18	55
Cr	Cr52	ppm	5770	4140	5320	5350	5930	5190	3530	4950	96	1560	200	54	191	9	310	283	62	131	714	344	6740	264	5390	1632	467	4670
Mn	Mn55	ppm	660	1040	837	625	871	679	1170	1040	1330	1310	1400	1400	1490	1340	640	736	492	342	619	717	529	702	490	423	479	458
Co	Co59	ppm	22	45	32	24	33	21	60	48	165	116	134	157	157	161	117	128	116	87	99	107	89	101	93	91	102	82
Ni	Ni60	ppm	454	637	555	472	413	348	1080	844	2630	1900	2380	2810	2840	2550	5732	6293	2233	1902	2998	5135	1738	4585	1960	3480	2550	1220
Cu	Cu63	ppm	1.8	2.2	2.4	1.9	2.4	1.7	4.7	3.4	1.9	8.2	6.6	1.5	4.2	0.4	28	67	8	12	15	45	19	72	11	56	44	6
Zn	Zn66	ppm	9	10	13	10	14	10	17	14	35	28	31	38	34	35	26	28	18	15	21	31	15	23	24	24	20	20
														oxides														
SiO_2	Si30	wt. %	48.8	45.6	47.9	48.3	50.3	49.8	48.7	48.8	39.0	43.1	39.1	38.0	39.0	35.7	42.2	45.2	43.4	42.8	46.5	44.9	43.7	46.2	43.2	46.2	46.4	44.3
Al_2O_3	Al27	wt. %	1.9	1.3	1.2	1.9	1.3	2.2	1.8	2.1	0.04	1.3	0.55	0.06	0.29	0.00	0.47	0.40	0.39	0.40	0.79	0.56	3.8	0.61	0.85	0.69	0.60	0.77
Cr_2O_3	Cr52	wt. %	0.84	0.61	0.78	0.78	0.87	0.76	0.52	0.72	0.01	0.23	0.03	0.01	0.03	0.00	0.05	0.04	0.01	0.02	0.10	0.05	0.98	0.04	0.79	0.24	0.07	0.68
TiO_2	Ti49	wt. %	0.02	0.01	0.02	0.02	0.02	0.03	0.10	0.11	0.00	0.01	0.01	0.00	0.01	0.00	0.02	0.01	0.01	0.01	0.01	0.01	0.02	0.02	0.02	0.02	0.02	0.02
MgO	Mg25	wt. %	26.8	37.0	30.8	26.6	32.6	26.4	32.2	29.1	50.1	49.3	50.8	51.1	51.9	53.6	53.8	50.1	52.5	53.7	50.2	51.0	47.7	49.9	52.5	49.8	49.2	51.4
MnO	Mn55	wt. %	0.09	0.13	0.11	0.08	0.11	0.09	0.15	0.13	0.17	0.17	0.18	0.18	0.19	0.17	0.08	0.09	0.06	0.04	0.08	0.09	0.07	0.09	0.06	0.05	0.06	0.06
FeO	Fe57	wt. %	1.5	2.7	1.8	1.5	1.9	1.6	4.8	4.4	10.6	6.0	9.5	10.8	8.7	10.7	3.5	4.3	3.8	3.2	2.5	3.6	3.8	3.3	2.8	3.2	3.8	3.0
CaO	Ca43	wt. %	20.0	12.8	17.4	20.6	13.0	19.0	11.8	14.6	0.29	0.03	0.02	0.03	0.02	0.01	0.02	0.02	0.00	0.00	0.01	0.02	0.01	0.02	0.02	0.04	0.02	0.02
Na_2O	Na23	wt. %	0.3	0.1	0.1	0.2	0.1	0.3	0.03	0.05	n.d.	n.d.	n.d.	n.d.	n.d.	n.d.	0.007	0.006	0.003	0.003	0.004	0.006	0.007	0.006	0.006	0.006	0.003	0.005
P_2O_5	P31	wt. %	0.002	0.002	0.002	0.003	0.004	0.003	0.003	0.003	0.004	0.002	0.002	0.004	0.006	0.002	0.004	0.012	0.004	0.002	0.003	0.004	0.002	0.003	0.005	0.005	0.005	0.004

[10] Most LA-ICP-MS analyses require an internal standard, which is an element whose concentration in the sample is known. Because the serpentinite matrices are heterogeneous, we could not a priori obtain an internal standard concentration for every ablation spot. For these reasons, all major and minor elements were analyzed. After elemental ratios were corrected using external standards, their oxides were assumed to sum to 100% (on an anhydrous level because volatiles were not analyzed). This approach allowed us to calculate the major and minor element concentrations of every ablation spot. The Si content determined in this way was then used as an internal standard to convert trace element signals into concentrations (Figure 2c). The accuracies of our major element compositions are within 5% (Figure 2d) for glasses and ultramafic minerals (olivine and pyroxene), indicating that our multistandard calibrations reduce matrix biases sufficiently for investigating fine-grained ultramafic materials, such as serpentine. One concern in analyzing serpentinite matrices is the high degree of heterogeneity. To minimize heterogeneity effects, we used a 110 micron spot size for the laser. Figures 2a and 2b represent examples of an ablation analysis of a serpentinized pyroxene. Relatively constant internal standard-normalized signal ratios as a function of time signify relative homogeneity on the 110 micron scale (Figure 2b). In some cases, $^{11}B/^{30}Si$ ratios are not constant with time. Such cases are likely to be the result of surface contamination of the thin section; these data were discarded or remeasured after washing the thick section again by ultrasonication with ethanol.

[11] Detection limits for the analytical protocols described above are as follows. For Li, detection limits (defined as 3 times the standard deviation of the blank background signal divided by the sensitivity) were 0.01 ppm. This is sufficiently low to investigate Li in ultramafic minerals and serpentinites. Detection limits for B were more difficult to assess. On the basis of the blank backgrounds, the theoretical detection limits for B were 0.1 ppm. However, when we analyzed standard reference materials with B contents known to be less than 1 ppm, we consistently obtained B concentrations in the range of 1–1.5 ppm. Thus, we consider 1.5 ppm to be the true detection limit of B for our laser ablation setup. The difficulty in analyzing low B concentrations is well-known [*Marschall and Ludwig*, 2004]. These poor detection limits are usually attributed to surface contamination of the samples themselves. We believe this is not the case in our samples because our samples have been repeatedly cleaned. Instead, we suspect that during laser ablation, B is liberated from the sample tubing (which contains a memory of previous B measurements) connecting the laser ablation cell to the ICP-torch because replacement of this tubing with clean tubing appears to decrease detection limits slightly. Sticky B on the tubing apparently is not liberated when simply running a gas background without ablation. The high B detection limits prevent us from measuring the B contents of primary ultramafic minerals, such as olivines, as B contents in olivines are often below 0.1 ppm [*Kent and Rossman*, 2002; *Herd et al.*, 2004; *Ottolini et al.*, 2004; *Kaliwoda et al.*, 2008]. For this study, however, the B contents in the serpentine minerals and moderately altered olivines and pyroxenes were well above our detection limit of 1.5 ppm. Finally, in addition to individual ablation spots, we also ran several laser traverses across the samples. Laser operating conditions and spot sizes were as described above, but the laser was swept across a predefined transect at 8 microns per second. In order to smooth out the data, every three consecutive instrument measurements (magnet scans) were averaged and treated as one measurement. Raw signals were converted into concentrations as described above. Examples of laser traverses are shown in Figure 3.

[12] External precision for individual spot measurements and traverse measurements are difficult to quantify because the heterogeneous nature of the samples precluded us from analyzing the same material repeatedly. Internal precision (standard error; SE) for a spot analysis is determined first by calculating the standard deviation of the ratio between the background-corrected count rates of the element of interest normalized to the count rate of the internal standard and then dividing this standard deviation by the square root of the number of measurements in a given laser run (typically 30–40). For most elements, including B and Li, the precision was within 5% (2 SE). Internal precision for laser traverses were calculated in the same way as spot measurements by averaging three consecutive measurements and taking the standard deviation of the three measurements. Precision for laser traverse measurements were at least an order of magnitude poorer than spot measurements (2SE for Li $\sim$ 40%, B $\sim$ 30%).

[13] Whole-rock data are compiled from *Agranier et al.* [2007] for B and from *Li and Lee* [2006] for major elements and all other trace elements. Ana-

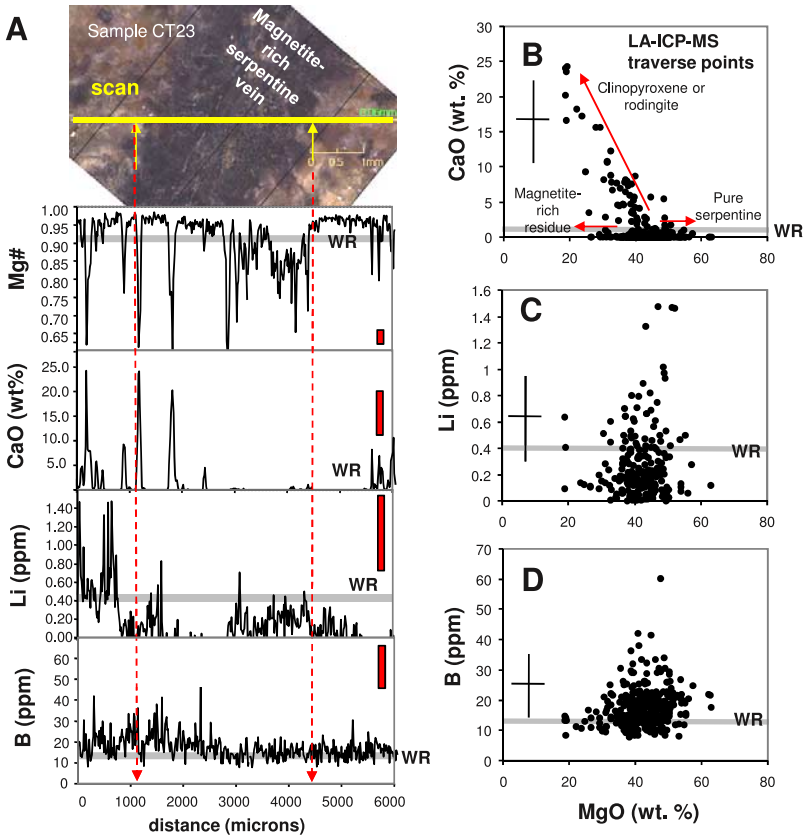

Figure 3. An example of one line traverse across a serpentinite vein. (a) Mg # (molar Mg/(Mg + Fe), CaO, Li, and B contents plotted as a function of distance (map of thick section scan shown at top). (b–d) Data from the traverses (every three consecutive measurements are averaged), showing CaO (Figure 3b), Li (Figure 3c), and B (Figure 3d) versus wt. % MgO. Arrows point to serpentine-rich zones, magnetite-rich zones, and Ca-rich zones (rodingites). Horizontal gray lines represent whole-rock composition for comparison. Vertical red bars in Figure 3a represent 2 standard error of traverse measurements. Crosses in Figures 3b–3d represent 2 standard error uncertainties of traverse measurements.

lytical details and uncertainties are provided in those papers.

4. Results

4.1. Line Traverses

[14] In Figure 3a, we provide an example of a line traverse (sample CT23) across a dark serpentinite vein (data for line scans in CT23 and CT10 are shown in the auxiliary material).[1] Every point in the line scan (each point represents the average of three consecutive measurements in the laser traverse) is also shown in Figures 3b–3c in the form of an element versus element plot. The darkness of the vein is caused by the presence of tiny magnetite crystals, which represent one of the byproducts of the serpentinization of olivine or pyroxene: serpentine minerals can only incorporate small amounts of Fe, so much of the original silicate-bound Fe is oxidized and converted into magnetite. These dark magnetite-rich veins represent zones where dissolved Fe was preferentially transported and precipitated, as evidenced by the low Mg # (<0.85) compared to the whole-rock Mg # of 0.9–0.91 (Mg # = molar Mg/(Mg + Fe)). In contrast, the borders of the veins are serpentine rich and characterized by very high Mg # (up to 0.95) due to loss of Fe to the veins during serpentinization. We also observed small (<1 mm) Fe-rich pockets that have no obvious association with magnetite-rich veins. The Fe-rich pockets are often associated with high Ca content (Figure 3b) and may represent local precipitation of Ca-bearing silicates from Ca- and Fe-rich fluids (serpentine minerals do not incorporate Ca into their structures); these Ca- and Fe-rich pockets might be microscopic analogs of rodingite veins. Li and B contents along the line scan are shown in Figure 3a. Li is generally depleted

[1]Auxiliary materials are available in the HTML. doi:10.1029/2008GC002078.

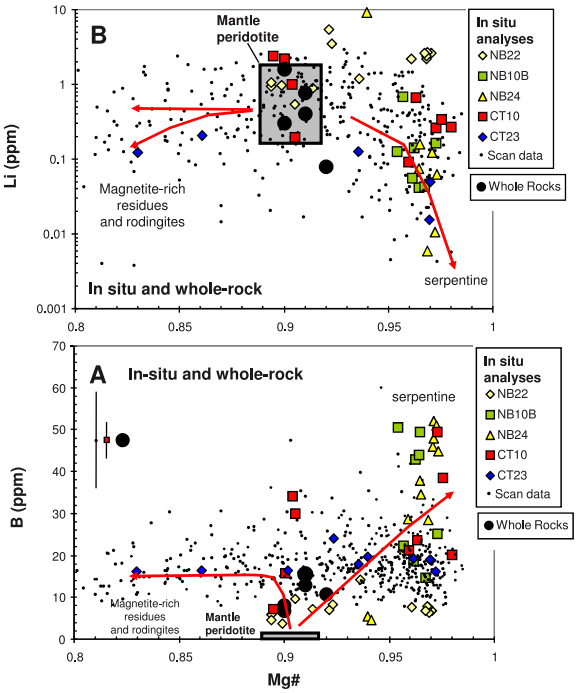

Figure 4. (a) B and (b) Li versus Mg # (molar Mg/(Mg + Fe)). Results of individual laser ablation spots are shown as large colored symbols for five different samples. Results of line scans from several samples are shown as small black dots. Large black dots represent whole-rock compositions corresponding to the samples investigated by laser ablation in this plot. Gray squares in Figures 4a and 4b represent estimated range of pristine, unaltered peridotite. Red arrows qualitatively represent the compositional effects of serpentinization. Vertical bars in Figure 4a represent 2 standard error uncertainties for traverse measurements, spot analyses, and whole rocks. Uncertainties in Figure 4b are not shown because of the log scale (see section 3 for discussion of uncertainties).

(<0.4 ppm) in the serpentinized veins or pockets relative to the whole rock (~0.4 ppm). In contrast, B is enriched in serpentine-rich zones (10–20 ppm) relative to relict olivine (<1 ppm [*Kent and Rossman*, 2002; *Kaliwoda et al.*, 2008], but there is no appreciable difference between whole-rock measurements and individual data points on the line scan. Individual (averaged of three passes) data points for other scans are shown in Figure 4.

4.2. Individual Spot Measurements

[15] The results of individual spot measurements for five different rock samples (NB22, NB10B, NB24, CT10 and CT23) are shown in Figure 4 (colored symbols) along with the combined results of line traverses from CT10, CT23 and NB10B (data are presented in Table 1). Whole-rock B and Li from *Agranier et al.* [2007] and *Li and Lee* [2006] corresponding to these samples are also shown for reference. We have denoted with a gray box the region corresponding to the B, Li, and Mg # expected for unaltered (e.g., not serpentinized or metasomatized) peridotites [*Ryan and Langmuir*, 1987; *Chaussidon and Jambon*, 1994; *McDonough and Sun*, 1995; *Leeman*, 1996; *Seitz and Woodland*, 2000; *Tomascak*, 2004; *Woodland et al.*, 2004]. Whole-rock Li contents (0.08–0.2) are similar or only slightly elevated with respect to unaltered peridotites (0.1–1 ppm). However, whole-rock B contents (~10 ppm) are elevated by at least an order of magnitude relative to unaltered peridotites (<1 ppm) [*Agranier et al.*, 2007]. Individual spot measurements for B show that serpentine minerals (identified by high Mg #, e.g., Mg # > 0.92) are very rich in B (up to 55 ppm), suggesting that the dominant hosts of B in the FRO serpentinites are the serpentine minerals themselves. In contrast, individual spot measurements of Li indicate that serpentine-rich zones often have Li contents lower than the unaltered peridotitic minerals. In a similar study by *Decitre et al.* [2002], most of the serpentinite minerals had higher Li contents than the relict minerals. However, in the FRO serpentinites, relict olivines and pyroxenes seem to hold as much and sometimes more Li than the serpentine minerals. Magnetite-rich zones (veins and rodingite pockets) do not seem to show any significant enrichments or depletions in B relative to the whole-rock.

5. Discussion

5.1. B Enrichment in Serpentinites

[16] The in situ and whole-rock B contents confirm that serpentine minerals are the dominant host of B in serpentinized rocks (Figures 1d and 3). The FRO peridotites, although serpentinized under much lower water/rock ratios than abyssal peridotites, have much lower whole-rock B contents (3–15 ppm) than serpentinized abyssal peridotites, which have hundreds of ppm B (Figure 1d) [*Savov et al.*, 2005a, 2005b]. The lower B contents of the FRO peridotites are due to lower initial B contents imparted by different styles of serpentinization (low water/rock ratio versus high water/rock ratio) or to loss of B during tectonic obduction onto the continent. Regardless of why the FRO peridotites have lower B contents than serpentinized abyssal peridotites, the B contents of the FRO peridotites are still much higher (by a factor of 10–20) than any estimates of

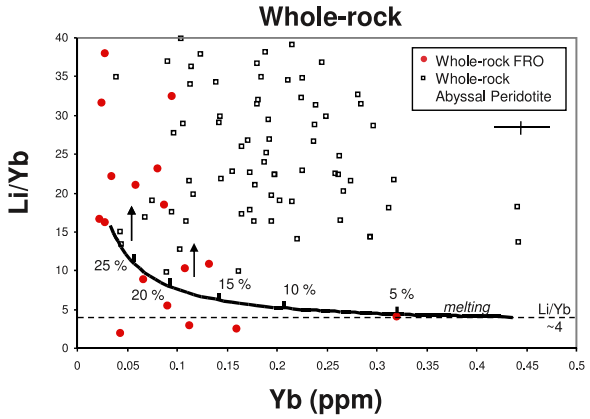

Figure 5. Li/Yb versus Yb in the whole-rock for abyssal peridotites [*Niu*, 2004] and FRO peridotites [*Li and Lee*, 2006]. Black curve represents calculated fractional melt depletion curve using partition coefficients described in the text. Tick marks represent melt fractions. Note Li/Yb rises with progressive melt extraction and clinopyroxene exhaustion. Cross represents 2 standard error uncertainties. Li/Yb of ~4 corresponds to Li/Yb of primitive mantle [*McDonough and Sun*, 1995].

the upper mantle's B content (<0.3 ppm [*McDonough and Sun*, 1995; *Leeman and Sisson*, 1996; *Ottolini et al.*, 2004]). According to *Tenthorey and Hermann* [2004] and *Scambelluri et al.* [2004], significant amounts of B may be retained in olivine during prograde metamorphism and dehydration of serpentine. High B contents in peridotites could thus signify a serpentinite protolith.

5.2. Variable Enrichments and Depletions in Li

[17] FRO whole-rock Li contents (~2 ppm) are lower to only slightly higher than estimates of the upper mantle [*McDonough and Sun*, 1995; *Leeman and Sisson*, 1996; *Ottolini et al.*, 2004] and are thus lower than serpentinized abyssal peridotites (>4 ppm; Figure 1c) [*Benton et al.*, 2004; *Niu*, 2004]. A similar result was found by *Decitre et al.* [2002] for oceanic peridotites from slow-spreading ridges: whole-rock Li contents were mostly <5 ppm. In any case, despite the lack of obvious enrichments in whole-rock Li, the FRO serpentinites have super-primitive mantle Li/Yb ratios (primitive mantle Li/Yb of 3–4 from *McDonough and Sun* [1995]) (Figure 5). In part, this could be because the whole-rock Yb contents in the FRO serpentinites are very low due to extensive (20–30%) melt depletion [*Li and Lee*, 2006]. Are the lower Li contents in the FRO peridotites compared to serpentinized abyssal peridotites due to preferential loss of Li during prograde metamorphic processes or are they low because of an initially lower enrichment in Li during the formation of serpentine? Our LA-ICP-MS measurements indicate that some serpentine minerals can have higher and lower Li than the host whole-rock and the less altered olivines (Figure 4), but for the most part, the relict olivines appear to retain most of the Li budget in the whole-rock. At face value, the low Li contents in some serpentine minerals seems peculiar as it implies that Li may have been locally leached out of the system during serpentinization (but net leaching is unlikely because Li contents in some samples are still higher than primitive mantle). In addition, in the study of *Decitre et al.* [2002], serpentine minerals tended to have higher concentrations of Li than relict olivines and pyroxenes, but they noted that some serpentine minerals had lower Li contents than relict olivines, particularly in the more harzburgitic lithologies. These observations collectively indicate that Li incorporation into serpentine minerals is complicated. One explanation is that Li has different affinities for serpentine minerals of different origin. Serpentine minerals can form from olivines, clinopyroxenes, and orthopyroxenes, but we were not able to distinguish confidently between the different serpentine origins due to the very fine-grained nature of these rocks. We speculate that the serpentine fractures and inclusions in the relict olivines are probably significant reservoirs of any secondary Li added to the peridotite during hydrothermal alteration.

[18] Like B, the Li contents in the FRO peridotites are clearly lower than abyssal peridotite B and Li contents. The important difference is that B contents of the FRO are still an order of magnitude higher than the B content of the mantle and thus indicate unequivocal enrichment (Figures 1d and 4a). However, the Li contents are no more than a factor of two higher than the Li content of model primitive mantle. Given that the FRO peridotites are harzburgites, it is reasonable to expect that they have experienced Li depletion during the high degrees of melt extraction required to generate harzburgites. If so, the relatively fertile levels of Li suggest that the harzburgites may have been slightly reenriched in Li. In section 5.3, we discuss how to quantify the level of Li reenrichment.

5.3. Detecting Li Enrichment Using Li/Yb-Yb Plots

[19] Because the Li enrichments in serpentinized ophiolitic rocks may be subtle, as exemplified by the FRO peridotites, detecting the Li enrichment

signal requires that we understand baseline Li contents imparted during partial melting processes in the mantle. Although it is commonly thought that the bulk partitioning behaviors of Li and Yb during mantle melting are similar (since Li/Yb ratios in primitive mid-ocean ridge basalts are constant and only slightly lower than that of primitive mantle), measurements of Li contents in peridotitic minerals indicate that olivine is the main carrier of Li [*Ryan and Langmuir*, 1987; *Seitz and Woodland*, 2000; *Ottolini et al.*, 2004]. On the basis of the Li contents in olivine, orthopyroxene, and clinopyroxene in spinel peridotite xenoliths, the mineral/melt partition coefficients follow the sequence: $D(Li)_{ol} > D(Li)_{opx} \sim D(Li)_{cpx}$ [*Seitz and Woodland*, 2000]. In contrast, clinopyroxene is the dominant host of Yb such that $D(Yb)_{cpx} > D(Yb)_{opx} > D(Yb)_{ol}$. Because progressive melt extraction leads to exhaustion of clinopyroxene and an increase in olivine proportion, the bulk partitioning (bulk partition coefficient is the average whole-rock/melt partition coefficient weighted according to the weight percent of each mineral mode) ratio of Li to Yb (D_{Li}/D_{Yb}) increases such that harzburgitic residues will eventually evolve to low Yb and Li contents, but more importantly to high Li/Yb ratios because Li becomes more compatible than Yb at higher degrees of melting. If Li/Yb is examined alone, the high Li/Yb ratios might give the impression of Li enrichment [*Ottolini et al.*, 2004]. The apparent similarity of Li and Yb behavior in mid-ocean ridge basalts is probably due to a coincidence of bulk partition coefficients at low melting degrees [*Ryan and Langmuir*, 1987], but the similarity breaks down once clinopyroxene is exhausted.

[20] To model the evolution of Li/Yb during melting, we adopted a fractional melting model with bulk partition coefficients, which varied as the mineralogy of the peridotitic residue (e.g., nonmodal) changed with progressive melt extraction (approximated from pMELTs [*Ghiorso et al.*, 2002] for isobaric 1.5 GPa melting; see Table 1 in the work of *Lee et al.* [2003] for modal abundances of minerals as a function of melting degree). The following mineral/melt partition coefficients for olivine (ol), orthoyroxene (opx), clinopyroxene (cpx), and spinel (sp) were assumed: $D(Li)_{ol} = 0.3$, $D(Li)_{opx} = 0.05$, $D(Li)_{cpx} = 0.10$, $D(Li)_{sp} = 0$ [*Seitz and Woodland*, 2000], $D(Yb)_{ol} = 0.015$, $D(Yb)_{opx} = 0.14$, $D(Yb)_{cpx} = 0.5$, and $D(Yb)_{sp} = 0$ [*Hauri et al.*, 1994; *Lee et al.*, 2007]. For a fertile lherzolite (opx = 28.1, cpx = 19.2, ol = 49.6, sp. = 3.1%), this yields bulk partition coefficients of 0.18 for Li and 0.14 for Yb, yielding $D_{Li}/D_{Yb} = 1.3$. Beyond 30% melting, wherein the residue is a clinopyroxene-free harzburgite (opx = 35.5, cpx = 0, ol = 62.9, sp. = 1.6%), the bulk partition coefficient is 0.22 for Li and only 0.05 for Yb, yielding $D_{Li}/D_{Yb} = 4.4$, which implies that Li becomes nearly 4 times more compatible than Yb.

[21] Figure 5 shows how Li/Yb varies with Yb in peridotite residues as a function of melting degree. Li/Yb ratios increase with increasing melt extraction implying that high Li/Yb ratios in peridotites do not by themselves indicate Li enrichment. Although our melting curve can be further refined with more accurate partitioning data, Figure 5 indicates that Li enrichment has occurred if the data in Li/Yb-Yb space plot above the melting curve. In the case of serpentinized abyssal peridotites [*Niu*, 2004], nearly all samples plot above the melt depletion line, implying unequivocal Li enrichment. In the case of the FRO peridotites, some of the harzburgitic lithologies have Li/Yb values plotting above the melt depletion line, but more fertile lithologies, such as lherzolites plot close to the melt depletion line. The apparent susceptibility of harzburgites to incompatible-element enrichment is commonly observed and is easily explained by the fact that the concentrations of incompatible trace elements like Li in harzburgites is very low, hence addition of even small amounts of contaminants have a large influence on the trace element composition of the harzburgite. Lherzolites are not as depleted in such elements and therefore are not as sensitive to contamination. We conclude from Figure 5 that some of the FRO peridotites have experienced secondary addition of Li after initial depletion by partial melt extraction. The fact that the Li/Yb ratios of these Li-reenriched harzburgites are far higher than typical MORBs, indicates that Li, not Yb, was preferentially introduced. This decoupling of Li from Yb suggests the involvement of aqueous fluids. In the case of the FRO, this is likely associated with serpentinization. In mantle xenoliths, high-temperature metasomatic effects would have to be considered.

[22] In conclusion, plots of whole-rock (or reconstructed whole-rock) Li/Yb versus Yb can be helpful in identifying whether Li enrichment has occurred in ultramafic lithologies, particularly in harzburgitic residues. In addition to serpentinization, there are many other ways to get secondary Li enrichments. For example, mesomatism by carbonatite melts and subduction-related fluids can give rise to Li enrichments [*Cooper et al.*, 1995; *Brenan*

et al., 1998a; *Brenan et al.*, 1998b; *Ottolini et al.*, 2004; *Halama et al.*, 2007].

6. Conclusions and Implications

[23] Feather River ophiolites (FRO) are enriched in B relative to unaltered peridotites, though not to the extent seen in abyssal peridotites. Serpentine minerals are highly enriched in B, indicating extensive introduction of B during serpentinization. In contrast, whole-rock Li contents in the FRO are relatively low compared to typical abyssal peridotites, which are thought to have undergone weathering serpentinization. In addition, serpentine minerals often have low Li contents compared to the whole-rock and unaltered peridotite minerals, which implies either that Li was lost during serpentinization or only small amounts were added. High whole-rock Li/Yb ratios in harzburgites can in part be explained by the increasing bulk compatibility of Li compared to Yb with progressive exhaustion of clinopyroxene and increase in olivine mode during partial melting. This implies that high Li/Yb ratios in ultramafic lithologies do not, by themselves, imply preferential metasomatic enrichment in Li. However, peridotite residues that plot above the Li/Yb versus Yb melt depletion curves may have experienced Li reenrichment (by serpentinization or other metasomatic processes) superimposed on a previous Li depletion associated with melt extraction. Recycling of serpentinites back into the mantle should generate a wide spectrum of B and Li elemental signatures owing to the large diversity of B and Li enrichments seen in serpentinites ranging from abyssal peridotites to oceanic lithospheric peridotites. However, if oceanic lithospheric peridotites, such as the Feather River Ophiolites, are the dominant types of serpentinite subducted back into the mantle, pronounced B enrichments and only subtle Li enrichments would be expected.

Acknowledgments

[24] This work was supported by NSF and Packard Foundation grants to Lee. We thank W. P. Leeman for obsidian glass standards. Most of the laser ablation analyses were done by Oka, whose summer undergraduate experience was supported by the above-mentioned funds. We are indebted to critical reviews by P. Tomascak and J. Ryan and the editorial suggestions of V. Salters.

References

Agranier, A., C.-T. A. Lee, X. A. Li, and W. P. Leeman (2007), Fluid mobile element budgets in serpentinized oceanic lithospheric mantle: Insights from B, As, Li, Pb, PGEs, and Os isotopes in the Feather River Ophiolite, California, *Chem. Geol.*, *245*, 230–241, doi:10.1016/j.chemgeo.2007.08.008.

Benton, L. D., J. G. Ryan, and I. P. Savov (2004), Lithium abundance and isotope systematics of forearc serpentinites, Conical Seamount, Mariana forearc: Insights into the mechanics of slab-mantle exchange during subduction, *Geochem. Geophys. Geosyst.*, *5*, Q08J12, doi:10.1029/2004GC000708.

Bonatti, E., J. R. Lawrence, and N. Morandi (1984), Serpentinization of oceanic peridotites: Temperature dependence of mineralogy and boron content, *Earth Planet. Sci. Lett.*, *70*, 88–94, doi:10.1016/0012-821X(84)90211-5.

Bostock, M., R. D. Hyndman, S. Rondenay, and S. M. Peacock (2002), An inverted continental Moho and serpentinization of the forearc mantle, *Nature*, *417*, 536–538, doi:10.1038/417536a.

Brenan, J. M., E. Neroda, C. C. Lundstrom, H. F. Shaw, F. J. Ryerson, and D. L. Phinney (1998a), Behavior of boron, beryllium, and lithium during melting and crystallization: Constraints from mineral-melt partitioning experiments, *Geochim. Cosmochim. Acta*, *62*, 2129–2141, doi:10.1016/S0016-7037(98)00131-8.

Brenan, J. M., F. J. Ryerson, and H. F. Shaw (1998b), The role of aqueous fluids in the slab-to-mantle transfer of boron, beryllium and lithium during subduction: Experiments and models, *Geochim. Cosmochim. Acta*, *62*, 3337–3347, doi:10.1016/S0016-7037(98)00224-5.

Brudzinski, M. R., C. H. Thurber, B. R. Hacker, and E. R. Engdahl (2007), Global prevalence of double Benioff zones, *Science*, *316*, 1472–1474, doi:10.1126/science.1139204.

Canil, D. (2008), Canada's craton: A bottoms-up view, *GSA Today*, *18*, 4–10, doi:10.1130/GSAT01806A.1.

Chaussidon, M., and A. Jambon (1994), Boron content and isotopic composition of oceanic basalts: Geochemical and cosmochemical implications, Earth Planet, *Sci. Lett.*, *121*, 277–291, doi:10.1016/0012-821X(94)90073-6.

Cooper, A. F., L. A. Paterson, and D. L. Reid (1995), Lithium in carbonatites - consequence of an enriched mantle source?, *Mineral. Mag.*, *59*, 401–408, doi:10.1180/minmag.1995.059.396.03.

Cooper, C. M., A. Lenardic, A. Levander, and L. Moresi (2006). Creation and preservation of cratonic lithosphere: Seismic constraints and geodynamic models, in *Archean Geodynamics and Environments*, *Geophys. Monogr. Ser.*, vol. 164, edited by K. Benn, J.-C. Mareschal, and K. C. Condie, pp. 75–88, AGU, Washington, D. C.

Day, H. W., E. M. Moores, and A. C. Tuminas (1985), Structure and tectonics of the northern Sierra Nevada, *Geol. Soc. Am. Bull.*, *96*, 436–450, doi:10.1130/0016-7606(1985)96<436:SATOTN>2.0.CO;2.

Decitre, S., E. Deloule, L. Reisberg, R. James, P. Agrinier, and C. Mevel (2002), Behavior of Li and its isotopes during serpentinization of oceanic peridotites, *Geochem. Geophys. Geosyst.*, *3*(1), 1007, doi:10.1029/2001GC000178.

Escartin, J., G. Hirth, and B. Evans (1997), Effects of serpentinization on the lithospheric strength and the style of normal faulting at slow-spreading ridges, *Earth Planet. Sci. Lett.*, *151*, 181–189, doi:10.1016/S0012-821X(97)81847-X.

Evans, B. W. (1977), Metamorphism of alpine peridotite and serpentinite, *Annu. Rev. Earth Planet. Sci.*, *5*, 397–447, doi:10.1146/annurev.ea.05.050177.002145.

Evans, B. W., J. Johannes, H. Oterdoom, and V. Trommsdorff (1976), Stability of chrysotile and antigorite in the serpentinite multisystem, *Schweiz. Mineral. Petrogr. Mitt.*, *56*, 79–93.

Gao, S., X. Liu, H. Yuan, B. Hattendorf, D. Günther, L. Chen, and S. Hu (2002), Determination of forty two major and trace elements in USGS and NIST SRM glasses by laser ablation-inductively coupled plasma-mass spectrometery, *Geostand. Newsl.*, *26*, 181–196, doi:10.1111/j.1751-908X.2002.tb00886.x.

Gao, Y., J. Hoefs, R. Przybilla, and J. E. Snow (2006), A complete oxygen isotope profile through the lower oceanic crust, ODP Hole 735B, *Chem. Geol.*, *233*, 217–234, doi:10.1016/j.chemgeo.2006.03.005.

Ghiorso, M. S., M. M. Hirschmann, P. W. Reiners, and V. C. Kress (2002), The pMELTS: A revision of MELTS for improved calculation of phase relations and major element partitioning related to partial melting of the mantle to 3 GPa, *Geochem. Geophys. Geosyst.*, *3*(5), 1030, doi:10.1029/2001GC000217.

Grove, T. L., N. Chatterjee, S. W. Parman, and E. Medard (2006), The influence of H2O on mantle wedge melting, *Earth Planet. Sci. Lett.*, *249*, 74–89, doi:10.1016/j.epsl.2006.06.043.

Hacker, B. R., and S. Peacock (1990), Comparison of the Central Metamorphic Belt and Trinity terrane of the Klamath mountains with the Feather River terrane of the Sierra Nevada, *Geol. Soc. Am. Spec. Pap.*, *255*, 75–92.

Hacker, B. R., S. M. Peacock, G. A. Aber, and D. Holloway (2003), Subduction factory 2. Are intermediate-depth earthquakes in subducting slabs linked to metamorphic dehydration reactions?, *J. Geophys. Res.*, *108*(B1), 2030, doi:10.1029/2001JB001129.

Halama, R., W. F. McDonough, R. L. Rudnick, J. Keller, and J. Klaudius (2007), The Li isotopic composition of Oldoinyo Lengai: Nature of the mantle sources and lack of isotopic fractionation during carbonatite petrogenesis, *Earth Planet. Sci. Lett.*, *254*, 77–89, doi:10.1016/j.epsl.2006.11.022.

Hauri, E. H., T. P. Wagner, and T. L. Grove (1994), Experimental and natural partitioning of Th, U, Pb and other trace elements between garnet, clinopyroxene and basaltic melts, *Chem. Geol.*, *117*, 149–166, doi:10.1016/0009-2541(94)90126-0.

Herd, C. D. K., A. H. Treiman, G. A. McKay, and C. K. Shearer (2004), The behavior of Li and B during planetary basalt crystallization, *Am. Mineral.*, *89*, 832–840.

Hilairet, N., B. Reynard, Y. Wang, I. Daniel, S. Merkel, N. Nishiyama, and S. Petitgirard (2007), High-pressure creep of serpentine, interseismic deformation, and initiation of subduction, *Science*, *318*(5858), 1910–1913.

Hirth, G., and D. L. Kohlstedt (1996), Water in the oceanic upper mantle; implications for rheology, melt extraction and the evolution of the lithosphere, *Earth Planet. Sci. Lett.*, *144*(1–2), 93–108, doi:10.1016/0012-821X(96)00154-9.

Hirth, G., and D. L. Kohlstedt (2004), Rheology of the upper mantle and the mantle wedge: A view from the experimentalists, in *Inside the Subduction Factory, Geophys. Monogr. Ser.,* vol. 138, edited by J. Eiler, pp. 83–106, AGU, Washington, D. C.

Janecky, D. R., and W. E. Seyfried, Jr. (1986), Hyrothermal serpentinization of peridotite within the oceanic crust: Experimental investigations of mineralogy and major element chemistry, *Geochim. Cosmochim. Acta*, *50*, 1357–1378, doi:10.1016/0016-7037(86)90311-X.

Kaliwoda, M., T. Ludwig, and R. Altherr (2008), A new SIMS study of Li, Be, B and δ^7Li in mantle xenoliths from Harrat Uwayrid, *Lithos*, doi:10.1016/j.lithos.2008.1007.1009, in press.

Kent, A. J. R., and G. R. Rossman (2002), Hydrogen, lithium, and boron in mantle-derived olivine: The role of coupled substitutions, *Am. Mineral.*, *87*, 1432–1436.

Lee, C.-T. A., and W.-P. Chen (2007), Possible density segregation of subducted oceanic lithosphere along a weak serpentinite layer and implications for compositional stratification of the Earth's mantle, *Earth Planet. Sci. Lett.*, *255*, 357–366, doi:10.1016/j.epsl.2006.12.022.

Lee, C.-T. A., A. D. Brandon, and M. D. Norman (2003), Vanadium in peridotites as a proxy for paleo-fO_2 during partial melting: Prospects, limitations, and implications, *Geochim. Cosmochim. Acta*, *67*(16), 3045–3064, doi:10.1016/S0016-7037(03)00268-0.

Lee, C.-T. A., A. Harbert, and W. P. Leeman (2007), Extension of lattice strain theory to mineral/mineral rare-earth element partitioning: An approach for assessing disequilibrium and developing internally consistent partition coefficients between olivine, orthopyroxene, clinopyroxene, and basaltic melt, *Geochim. Cosmochim. Acta*, *71*, 481–496, doi:410.1016/j.gca.2006.1009.1014.

Lee, C.-T. A., P. Luffi, T. Höink, Z.-X. A. Li, and A. Lenardic (2008), The role of serpentine in preferential craton formation in the late Archean by lithosphere underthrusting, *Earth Planet. Sci. Lett.*, *269*, 96–104, doi:10.1016/j.epsl.2008.02.010.

Leeman, W. P. (1996), Boron and other fluid-mobile elements in volcanic arc lavas: Implications for subduction processes, in *Subduction Top to Bottom, Geophys. Monogr. Ser.*, vol. 96, edited by G. E. Bebout et al., pp. 269–276, AGU, Washington, D. C.

Leeman, W. P., and V. B. Sisson (1996), Geochemistry of boron and its implications for crustal and mantle processes, in *Boron: Mineralogy, Petrology and Geochemistry in the Earth's Crust*, edited by E. S. Grew and L. M. Anovitz, pp. 645–707, Mineral. Soc. of Am., Chantilly, Va.

Li, Z.-X. A., and C.-T. A. Lee (2006), Geochemical investigation of serpentinized oceanic lithospheric mantle in the Feather River Ophiolite, California: Implications for the recycling rate of water by subduction, *Chem. Geol.*, *235*, 161–185, doi:10.1016/j.chemgeo.2006.06.011.

Marschall, H. R., and T. Ludwig (2004), The low-boron contest: Minimising surface contamination and analysing boron concentrations at the ng/g-level by secondary ion mass spectrometry, *Mineral. Petrol.*, *81*, 265–278, doi:10.1007/s00710-004-0037-5.

Mayfield, J. D., and H. W. Day (2000), Ultramafic rocks in the Feather River Belt, northern Sierra Nevada, in *Field Guide to the Geology and Tectonics of the Northern Sierra Nevada*, edited by E. R. Brooks and L. T. Dida, pp. 1–15, Calif. Div. of Mines and Geol., Sacramento.

McDonough, W. F., and S.-S. Sun (1995), The composition of the Earth, *Chem. Geol.*, *120*, 223–253, doi:10.1016/0009-2541(94)00140-4.

Niu, Y. (2004), Bulk-rock major and trace element compositions of abyssal peridotites: Implications for mantle melting, melt extraction and post-melting processes beneath mid-ocean ridges, *J. Petrol.*, *45*, 2423–2458, doi:10.1093/petrology/egh068.

Ottolini, L., B. Le Fevre, and R. Vannucci (2004), Direct assessment of mantle boron and lithium contents and distribution by SIMS analyses of peridotite minerals, *Earth Planet. Sci. Lett.*, *228*, 19–36, doi:10.1016/j.epsl.2004.09.027.

Ranero, C. R., J. Phipps Morgan, K. McIntosh, and C. Reichert (2003), Bending-related faulting and mantle serpentinization at the Middle America trench, *Nature*, *425*, 367–373, doi:10.1038/nature01961.

Rüpke, L. H., J. P. Morgan, M. Hort, and J. A. D. Connolly (2004), Serpentine and the subduction zone water cycle,

Earth Planet. Sci. Lett., *223*, 17–34, doi:10.1016/j.epsl.2004.04.018.

Ryan, J. G., and C. H. Langmuir (1987), The Systematics of Lithium Abundances in Young Volcanic-Rocks, *Geochim Cosmochim. Acta*, *51*(6), 1727–1741, doi:10.1016/0016-7037(87)90351-6.

Savov, I. P., S. Guggino, J. G. Ryan, P. Fyer, and M. J. Mottle (2005a), Geochemistry of serpentinite muds and metamorphic rocks from the Mariana forearc, ODP Sites 1200 and 778–770, South Chamorro and Conical seamounts, *Proc. Ocean Drill. Program, Sci. Results*, *195*, 1–49.

Savov, I. P., J. G. Ryan, M. D'Antonio, K. Kelley, and P. Mattie (2005b), Geochemistry of serpentinized peridotites from the Mariana forearc conical seamount, ODP Leg 125: Implications for the elemental recycling at subduction zones, *Geochem. Geophys. Geosyst.*, *6*, Q04J15, doi:10.1029/2004GC000777.

Scambelluri, M., P. Bottazzi, V. Trommsdorff, R. Vannucci, J. Hermann, M. T. Gomez-Pugnaire, and V. L.-S. Vizcaino (2001), Incompatible element-rich fluids released by antigorite breakdown in deeply subducted mantle, *Earth Planet Sci. Lett.*, *192*, 457–470, doi:10.1016/S0012-821X(01)00457-5.

Scambelluri, M., O. Müntener, L. Ottolini, T. T. Pettke, and R. Vannucci (2004), The fate of B, Cl, and Li in subducted oceanic mantle and in the antigorite breakdown fluids, *Earth Planet. Sci. Lett.*, *222*, 217–234, doi:10.1016/j.epsl.2004.02.012.

Seitz, H.-M., and B. J. Woodland (2000), The distribution of lithium in peridotitic and pyroxenitic mantle lithologies - an indicator of magmatic and metasomatic processes, *Chem. Geol.*, *166*, 47–64, doi:10.1016/S0009-2541(99)00184-9.

Seyfried, W. E., Jr., and W. E. Dibble Jr. (1980), Seawater peridotite interaction, an experimental study at 300°C, 500 bars: Implications for the origin of oceanic serpentinites, *Geochim. Cosmochim. Acta*, *44*, 309–321, doi:10.1016/0016-7037(80)90139-8.

Seyfried, W. E., X. Chen, and L.-H. Chan (1998), Trace element mobility and lithium isotope exchange during hydrothermal alteration of seafloor weathered basalt: An experimental study at 350°C, 500 bars, *Geochim. Cosmochim. Acta*, *62*, 949–960, doi:10.1016/S0016-7037(98)00045-3.

Snow, J. E., and H. J. B. Dick (1995), Pervasive magnesium loss by marine weathering of peridotite, *Geochim. Cosmochim. Acta*, *59*, 4219–4235, doi:10.1016/0016-7037(95)00239-V.

Tenthorey, E., and J. Hermann (2004), Composition of fluids during serpentinite breakdown in subduction zones: Evidence for limited boron mobility, *Geology*, *32*, 865–868, doi:10.1130/G20610.1.

Tomascak, P. B. (2004), Developments in the understanding and application of lithium isotopes in the Earth and planetary sciences, in *Geochemistry of Non-Traditional Stable Isotopes*, edited by C. Johnson, B. Beard, and F. Albarede, pp. 153–195, Mineral. Soc. of Am., Washington, D. C.

Woodland, A. B., H.-M. Seitz, and G. M. Yaxley (2004), Varying behaviour of Li in metasomatised spinel peridotite xenoliths from western Victoria, Australia, *Lithos*, *75*, 55–56, doi:10.1016/j.lithos.2003.12.014.